Evidence for the stability of ultrahydrous stishovite in Earth's lower mantle HPSTAR 874-2019

Yanhao Lin[a,1], Qingyang Hu[b,1], Yue Meng[c], Michael Walter[a], and Ho-Kwang Mao[b,1]

[a]Geophysical Laboratory, Carnegie Institution for Science, Washington, DC 20015; [b]Center for High Pressure Science and Technology Advanced Research, Shanghai 201203, People's Republic of China; and [c]High-Pressure Collaborative Access Team (HPCAT), X-Ray Science Division, Argonne National Laboratory, Lemont, IL 60439

Contributed by Ho-Kwang Mao, November 20, 2019 (sent for review August 19, 2019; reviewed by Arianna E. Gleason and Jin S. Zhang)

The distribution and transportation of water in Earth's interior depends on the stability of water-bearing phases. The transition zone in Earth's mantle is generally accepted as an important potential water reservoir because its main constituents, wadsleyite and ringwoodite, can incorporate weight percent levels of H_2O in their structures at mantle temperatures. The extent to which water can be transported beyond the transition zone deeper into the mantle depends on the water carrying capacity of minerals stable in subducted lithosphere. Stishovite is one of the major mineral components in subducting oceanic crust, yet the capacity of stishovite to incorporate water beyond at lower mantle conditions remains speculative. In this study, we combine in situ laser heating with synchrotron X-ray diffraction to show that the unit cell volume of stishovite synthesized under hydrous conditions is ∼2.3 to 5.0% greater than that of anhydrous stishovite at pressures of ∼27 to 58 GPa and temperatures of 1,240 to 1,835 K. Our results indicate that stishovite, even at temperatures along a mantle geotherm, can potentially incorporate weight percent levels of H_2O in its crystal structure and has the potential to be a key phase for transporting and storing water in the lower mantle.

ultrahydrous stishovite | water transporting | deep mantle | high pressure–temperature

Liquid water covering Earth's surface is a unique feature among the terrestrial planets. Plate tectonics, through the continuous subduction of rocks that have interacted with the surface hydrosphere, may regulate surface water through a deep water cycle that involves mineral phases capable of storing water at the high-pressure and -temperature conditions of Earth's mantle. The presence of water in the mantle can affect significantly the chemical and physical properties of the rock-forming minerals, including mineral phase relations, melting temperatures, rheological properties, electrical conductivity, and seismic velocities (1–9). Water transport and storage in the mantle may also regulate the surface water reservoir over geological time through a deep water cycle.

Water is transported into the mantle at subduction zones in hydrous phases (10–13), in nominally anhydrous minerals (14–18), or as a fluid captured in disconnected interstitial patches in mantle rocks (19). In basaltic oceanic crust and sediment, hydrous phases destabilize at the temperatures of the slab top during subduction with models indicating nearly complete dehydration by ∼200 km (20), leading to melting in the mantle wedge that produces primary arc magmas with an average of ∼4 wt % H_2O (21). Hydrous phases (e.g., serpentine, chlorite, clinohumite, chondrodite) and dense hydrous magnesium silicates (DHMSs; DHMS phases: Phase A, superhydrous B, D, and H) that are stable in the peridotitic portion of the lithosphere can potentially transport significant quantities of water into the deeper mantle in colder subducting slabs but are predicted to destabilize either within the transition zone or on entry into the lower mantle, and they are certainly not stable at the temperatures of the mantle geotherm (11, 13, 22, 23). This deeper mantle dehydration of the slab perhaps makes the transition zone the largest potential reservoir for water in Earth's mantle because its main constituent minerals, wadsleyite and ringwoodite, can incorporate up to ∼1 to 1.5 wt % H_2O in their structures at mantle temperature (24).

The potential for water to be transported and remain stable in minerals in the deeper, lower mantle will depend on the capacity of nominally anhydrous minerals to incorporate water into their structures. Here, we focus on the mineral stishovite, a high-pressure polymorph of silica (SiO_2) that is a major component of subducted oceanic crust (∼23% by volume) (25, 26). Up to ∼9 GPa (∼300 km), all forms of silica, like quartz, are built up of SiO_4 tetrahedra, with coesite being the highest-pressure polymorph of this type. At higher pressures, stishovite, a tetragonal phase with a rutile structure ($P4_2/mnm$) and with silicon in octahedral coordination with oxygen, is stable up to ∼70 GPa along a mantle geotherm, where it transforms through a second-order displacive phase transition to an orthorhombic $CaCl_2$-structured phase (27–29). Recent high-pressure experiments have shown up to ∼3.2 wt % H_2O in stishovite synthesized at ∼10 GPa and 723 K (18, 30), a temperature far too low to be appropriate for Earth's mantle. If such quantities of water can be accommodated at higher pressures and temperatures, stishovite may become a potentially important phase for subducting water into the deeper mantle. Here, we investigate whether such large amounts of water can be accommodated by stishovite at high temperatures and pressures appropriate for the mantle beyond the transition zone (∼27 to 58 GPa and ∼1,240 to 1,835 K).

Results and Discussion

The starting material for our experiments was a mixture of amorphous SiO_2 and goethite (α-FeOOH) in the molar ratio of

Significance

The great abundance of water on Earth's surface makes it different from other terrestrial planets, and it may be linked to a deep interior water cycle. How water is transported into Earth's deep interior and in which phases it is held are still a matter of much debate. Stishovite is known as a major component of subducted oceanic basalt, and recent experiments have reported that it can incorporate significant amounts of water in its crystal structure. Here, we show that, at the pressure–temperature conditions of a mantle geotherm, stishovite may be a key phase for transporting water into the deep mantle, providing important information on the water cycle in the deep earth.

Author contributions: Y.L., Q.H., M.W., and H.-K.M. designed research; Y.L., Q.H., Y.M., M.W., and H.-K.M. performed research; Y.L., Q.H., Y.M., and M.W. analyzed data; and Y.L., Q.H., M.W., and H.-K.M. wrote the paper.

Reviewers: A.E.G., SLAC National Accelerator Laboratory; and J.S.Z., University of New Mexico.

The authors declare no competing interest.

[1]To whom correspondence may be addressed. Email: yhlin@carnegiescience.edu, qingyang.hu@hpstar.ac.cn, or maohk@hpstar.ac.cn.

This article contains supporting information online at https://www.pnas.org/lookup/suppl/doi:10.1073/pnas.1914295117/-/DCSupplemental.

4:1, with goethite serving as a source of water. About 2 wt % Pt black powder was added to the mixture for infrared laser absorption in laser-heating experiment (*Methods* has more details). The sample assembly consisted of the SiO_2–goethite mixture sandwiched between 2 layers of amorphous SiO_2 (*Methods*). The sample was first compressed to ∼30 GPa (Run 1) at room temperature. We used both ruby and Pt as internal pressure standards (*Methods* has details). The sample was then heated using a double-sided laser system and held at target temperatures for ∼10 min each: 1,240 K at 32.5 GPa (27 GPa), 1,450 K at 33.1 GPa (34 GPa), and 1,775 K at 34 GPa (37 GPa), where Pt pressures are in parentheses. In situ X-ray diffraction (XRD) spectra were acquired at each pressure and temperature condition and also, after quenching to ambient temperature. Subsequently, the sample was compressed to 39 GPa (Run 2) at room temperature and then heated in a different location to temperatures of 1,310 K at 48.3 GPa (37 GPa), 1,410 K at 49 GPa (52 GPa), and 1,835 K at 52 GPa (58 GPa). The diffraction data show that our heated sample was dominated by stishovite with a minor amount of Fe_2O_3 and FeOOH in the high-pressure ε phase (Fig. 1). At high pressure and 300 K, we find that sharp diffraction lines agree well with the expected diffraction pattern of anhydrous stishovite (31), except that they are systematically shifted to higher *d* spacings. Unit cell parameters acquired at 300 K and high pressure are summarized in Fig. 2 and Table 1. The much larger volumes of stishovite synthesized under hydrous conditions relative to volumes of anhydrous stishovite calculated from its equation of state at the same pressures (29, 31, 32) provide primary evidence for considerable hydration.

Spektor et al. (18, 33) and Nisr et al. (30) reported on the synthesis of hydrous Al-free stishovite samples grown at 9 and 10 GPa under hydrothermal, low-temperature conditions (350 °C to 550 °C). The water content of their samples was calibrated based on thermogravimetric analysis and secondary ion mass spectrometry, with reported water contents of up to 3.2 wt % H_2O. These authors suggest H incorporation into SiO_2 through an octahedral "hydrogarnet"-type defect mechanism with hydroxyl groups around a silicon vacancy, equivalent to direct cation substitution of the form $4H^+ \rightarrow Si^{4+}$ (18, 30). Spektor et al. (33) provided a calibration for the water content of stishovite on the basis of the observed volume change relative to anhydrous stishovite in samples quenched to 1 bar and 300 K. To make an initial estimate of the water content in our samples, we assume that the slope of the observed linear relationship at 1 bar is constant with pressure and use the equation of state of Andrault et al. (31) to determine the volume of anhydrous stishovite at high pressure. On this basis, the changes in unit cell volume observed in our study would indicate about 4.5 to 10 wt % H_2O in stishovite at high pressure (Table 1). However, this approach may not be reliable if the compression behaviors of hydrous and anhydrous stishovite are different. Nisr et al. (34) measured the equation of state of hydrous stishovite with ∼3.2 wt % H_2O, which is shown relative to the equation of state of anhydrous stishovite on Fig. 2. The higher compressibility of hydrous stishovite indicates that the change in volume at higher pressures with the addition of H_2O is expected to be less than at 1 bar as shown in Fig. 2. Thus, our estimates based on the 1-bar data would be minimal. On the basis of a linear extrapolation of the difference in observed bulk moduli from these studies (31, 34) to higher water contents, our samples could contain as much as 10 wt % or more H_2O (Fig. 2).

When using the ruby pressure calibration, where the ruby was off center to the heated area, the results apparently indicate that the water contents in stishovite are very high (e.g., 10 wt % H_2O or more) but decrease systematically with temperature. However, when using the Pt pressure calibration, where the Pt is in the same location as the X-ray spot, the data fan out nearly parallel to a compression curve, possibly indicating synthesis of stishovite with a relatively constant but still very high water content (Table 1). The remarkably high water content predicted for our stishovite samples based on the volume change may be explicable when considering that other rutile-structured high-pressure hydrous phases, like δ-AlOOH and Phase H ($MgSiH_2O_4$), contain ∼15 wt % H_2O in their structures. We note that Phase H becomes stable at ∼35 to 40 GPa in the MgO–SiO_2–H_2O system at the temperatures in our study (13). Whether or not the stishovite we observe is a fully hydrated stoichiometric phase or a high but limited solid solution remains an open question that we cannot address further with our data.

The extremely high amounts of water estimated for the stishovite samples in this study based on their expanded unit cell volumes are much higher than observed in any previous study (summarized in *SI Appendix*, Table S1). For example, the stishovite samples synthesized at ∼9 to 10 GPa and 723 K by Spektor et al. (18) (∼1.3 wt %) and Nisr et al. (30) (∼3.2 wt %) and at 15 GPa and 1,500 °C by Bolfan-Casanova et al. (14) (72 ppm) in the pure SiO_2 system have much lower water contents, especially at high temperature. Previous results have indicated that the incorporation of alumina (<2.3 wt % Al) in stishovite promotes the substitution of water in stishovite through the cation substitution mechanism ($Al^{3+} + H^+ \rightarrow Si^{4+}$), which includes the Al-bearing stishovites synthesized at 10 GPa and 1,200 °C by Pawley et al. (35) (82 ppm for 1.51 wt % Al_2O_3), 15 GPa and 1,400 °C by Chung and Kagi (36) (844 ppm for 1.32 wt % Al_2O_3), ∼32 GPa and 2,577 °C by Panero et al. (37) (∼460 ppm for 3 wt % Al_2O_3), and 20 GPa and 1,400 °C by Litasov et al. (17) (3,010 ppm for 4.4 wt % Al_2O_3).

Stishovite is not expected to be a stable phase in peridotite bulk compositions either in ambient mantle or in the mantle portion of subducted lithosphere (14, 38, 39). However, in subducted basaltic compositions, like midocean ridge basalt (MORB), stishovite becomes a modally abundant phase at transition zone depths where it coexists with majorite garnet. At lower mantle conditions, stishovite comprises ∼23 modal % in MORB, coexisting with aluminous bridgmanite (∼22 modal %), Na–Al phase phase (∼35 modal %), and Ca–ferrite-structured phase (∼20 modal %) (17). Among these nominally anhydrous phases in basaltic compositions at lower mantle pressures, stishovite stands out as a phase that can potentially contain a large amount of water while remaining stable along the mantle geotherm. In contrast, bridgmanite can accommodate perhaps 2 orders of magnitude less water (∼1,000 ppm water) (40), and there are no data on the water storage capacities of the Na–Al phase and Ca–ferrite phases.

Dense hydrous phases can also potentially be stable in basaltic compositions, like Phase D in the transition zone and upper lower mantle or Phase H in the midlower mantle to the base of the mantle (15). However, these phases are not stable along a mantle geotherm and would only stabilize at lower temperatures in cold slabs after the nominally anhydrous phases, like stishovite in oceanic crust, exceed their storage capacity (13). Because of its potential to store exceptionally large amounts of water at high temperatures, stishovite is potentially the most important host of water in basaltic compositions in the transition zone and lower mantle.

Subducted oceanic crust is considered to be largely dehydrated in the upper mantle (20). However, water may be subducted into the transition zone in the peridotitic lithosphere in postserpentine dense hydrous phases, like Phase A, superhydrous Phase B, or Phase D (41). These phases may break down in the transition zone if subducting lithosphere founders and heats up. The discovery of hydrous ringwoodite as an inclusion in "superdeep" diamond (42) as well as boron-rich diamonds originating from around 700-km depth (43) indicates that at least locally water-enriched regions of diamond formation may be linked to slab dehydration. Furthermore, seismic velocity anomalies observed in the uppermost lower mantle have been ostensibly attributed to the melting caused by dehydration of hydrous ringwoodite when it breaks down to

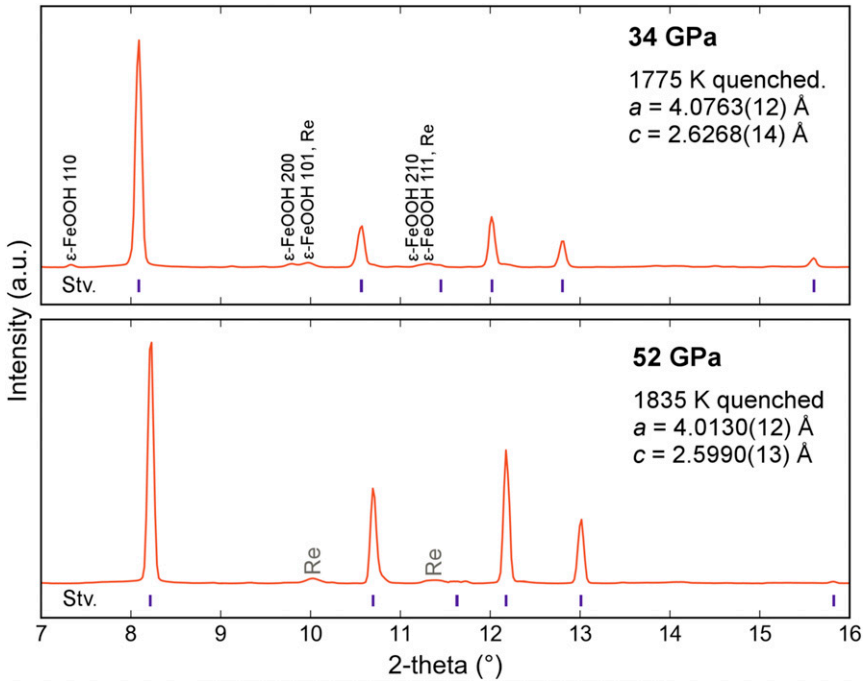

Fig. 1. XRD patterns at 34 and 52 GPa (ruby pressures) and 300 K after laser heating. At the center of the heated area, the majority of diffraction peaks belong to stishovite. The transition from stishovite to $CaCl_2$-type SiO_2 was not observed in our experiment. Data were acquired using an X-ray wavelength of 0.4066 Å.

nominally anhydrous bridgmanite and ferropericlase (6) or alternatively, due to melting caused by breakdown of Phase D or Phase H (13). These observations indicating release of water from subducted lithosphere via dehydration or hydrous melting also suggest that stishovite, even if it were effectively anhydrous in oceanic crust that had previously dehydrated, could become an important carrier for water into the lower mantle on rehydration (Fig. 3).

Water or hydrous melts from dehydration of ringwoodite or dense hydrous silicates in peridotitic subducted lithosphere in the transition zone or the upper lower mantle may infiltrate subducted basaltic oceanic crust where they can be accommodated in hydrous stishovite. With further subduction into the lower mantle, stishovite would remain stable, even if the slab heats up to the mantle geotherm. Stishovite undergoes a transition to $CaCl_2$-structered phase at ~70 GPa along a mantle geotherm, and it is not known if this phase can also accommodate abundant water (28). In addition, Lakshtanov et al. (5) suggested that the rutile–$CaCl_2$ transition pressure in stishovite with ~5 wt % Al_2O_3 can be as low as ~24 GPa. However, as the transition is second order resulting from a small distortion of the unit cell from tetragonal to orthorhombic with only a minor volume change (44), we predict it may also accommodate significant H through protonation.

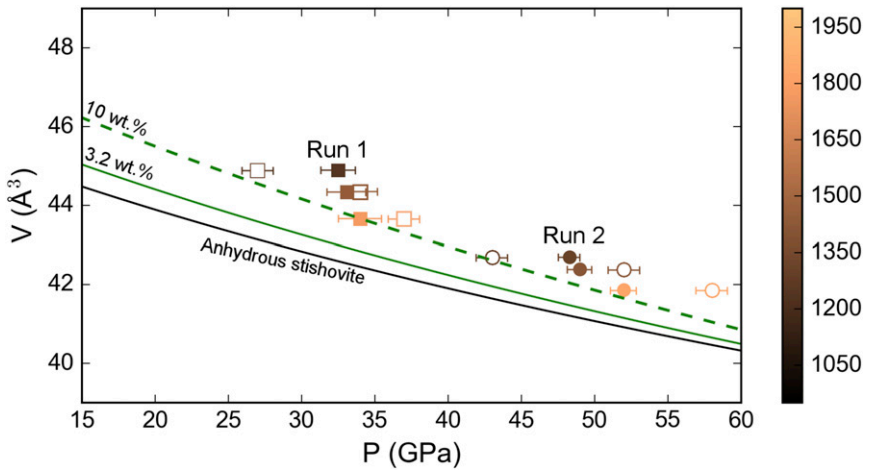

Fig. 2. Measured stishovite unit cell volumes at high pressure and 300 K. Solid squares (Run 1) and solid circles (Run 2) show pressure based on the ruby pressure calibration [the error bar based on stress anisotropy (51)], whereas open squares and open circles show pressure based on the Pt pressure calibration (the error bar of ±2 GPa). The solid black curve shows the equation of state for anhydrous stishovite of Andrault et al. (31). The solid green curve shows the equation of state of stishovite with 3.2 wt % H_2O from Nisr et al. (34). The dashed green line is an estimated equation of state for stishovite with 10 wt % H_2O on the basis of a linear extrapolation of the bulk moduli for the anhydrous stishovite and stishovite with 3.2% H_2O (31, 34). The decompression data are shown in *SI Appendix*, Fig. S3.

Table 1. Summary of experimental results

Experiment	T (K)	*a* (Å)	*c* (Å)	*V* (Å^3)	1 Sigma (Å^3)	Pressure by the ruby calibration				Pressure by the Pt calibration			
						P (GPa)	*V*(dry) (Å^3)	ΔV (Å^3)	C (H_2O, wt %)*	P (GPa)	*V*(dry) (Å^3)	ΔV (Å^3)	C (H_2O, wt %)*
Run1													
LH04	1,240 (50)	4.1337	2.6509	45.298	0.025	32.5							
LH05	300	4.1211	2.6426	44.879	0.025	32.5	42.752	2.127	9.9	27	43.285	1.594	7.4
LH06	1,255 (50)	4.1331	2.6474	45.224	0.025	32.5							
LH07	1,450 (60)	4.1156	2.6443	44.788	0.025	33.1							
LH08	300	4.1010	2.6357	44.329	0.025	33.1	42.695	1.634	7.6	34	42.606	1.723	8.0
LH09	1,775 (90)	4.0863	2.6388	44.062	0.024	34.0							
LH10	300	4.0763	2.6268	43.648	0.024	34.0	42.606	1.042	4.8	37	42.315	1.333	6.2
Run2													
LH11	300	4.0691	2.6255	43.473	0.024	39.0	42.121	1.352	6.3				
LH12	1,310 (50)	4.0515	2.6126	42.885	0.029	48.3							
LH13	300	4.0434	2.6109	42.686	0.023	48.3	41.221	1.466	6.8	43	41.733	0.953	4.4
LH14	1,410 (50)	4.0519	2.6104	42.857	0.024	49.0							
LH15	300	4.0289	2.6109	42.379	0.023	49.0	41.152	1.227	5.7	52	40.860	1.519	7.0
LH16	1,750 (90)	4.0207	2.6046	42.106	0.023	51.4							
LH17	1,835 (100)	4.0197	2.6036	42.070	0.023	52.0							
LH18	300	4.0130	2.5990	41.854	0.023	52.0	40.860	0.994	4.6	58	40.278	1.576	7.3

C, concentration; P, pressure; T, temperature.
*Water content is calculated by using the equation: C (H_2O, wt %) = 4.64 $\times \Delta V$ from Nisr et al. (30).

As a modally abundant phase in subducted oceanic crust, stishovite has the potential to transport a significant quantity of water into the deep mantle. Assuming current values for the average subduction rate (5 cm y^{-1}), length of subduction zones (46,000 km), and crustal thickness (6 km) (37), we estimate that, for an abundance of 23% in a subducted MORB, 4.6×10^{22} kg of stishovite would be subducted into the deep mantle per year. Although we cannot constrain the water content in deeply subducted oceanic crust, with the addition of each 1 wt % H_2O to stishovite, subducted oceanic crust could transport ~10^{11} kg of water per year into the deep mantle. To put that quantity into perspective, current estimates for the water content of the mantle are about 0.75 oceans masses based on geochemical arguments (45) or about 10^{21} kg. This entire quantity of water could be transported to the mantle by stishovite over 4 billion y of subduction if the average stishovite water content was ~2 wt %. If water in stishovite is partially released during the transportation, stishovite is requested to contain water more than ~2 wt % at the start to reach the geochemical estimation (45).

In conclusion, our results indicate that stishovite can accommodate weight percent levels of water in its structure. As a modally abundant phase in subducted oceanic crust, stishovite is a potential carrier of significant quantities of water into the deep earth even at the high temperatures along a mantle geotherm. Our results have not yet quantified precisely the storage capacity of water in stishovite in oceanic crustal assemblages, and more work is needed to understand how water partitions among coexisting phases as well as the thermodynamic and physical properties of hydrous stishovite (e.g., seismic velocities) as a function of temperature, pressure, and minor element concentrations (Al^{3+}, Fe^{3+}).

Methods

Starting Materials and Experimental Design. A mixture of SiO_2 (amorphous, 1-μm grain size, purity 99.999%), FeOOH (goethite), and Pt black were ground in a ball mill for 1.5 h. The starting material was cold pressed into a thin foil ~60 × 60 μm^2 in size and ~10 μm in thickness. The sample foil was loaded in a 150-μm-diameter hole in a rhenium gasket indented by diamond anvils with 200-μm culet diameter and embedded between 2 layers of SiO_2 that served as a thermal insulator and solid pressure medium in a symmetric diamond-anvil cell (46). We loaded a ruby chip peripheral to the sample on the cylinder side that was used as a pressure calibrant. Samples were heated in a double-sided laser-heated diamond-anvil cell and examined in situ at high pressures and temperatures by synchrotron X-ray powder diffraction at beamline 16-IDB of the Advanced Photon Source, Argonne National Laboratory (47). The X-ray beam size was 4.8 × 5.3 μm^2 with a wavelength of 0.4066 Å. For laser heating, the diameter of a laser-heating spot was up to ~40 μm at ~1,800 K in the flat top area created with a focused yttrium lithium fluoride laser using a double-sided heating technique that minimizes both radial and axial temperature gradients. Temperatures were determined by fitting the thermal radiation from the central portion of the heated spot to the Planck radiation function (48). The unit cell is calculated by indexing the 110, 101, 111, 210, and 211 diffraction peaks of stishovite by a nonlinear fitting program (details are in *SI Appendix*, Table S2) (49). Pressures were determined before and after heating using the calibrated ruby fluorescence line shift in an offline ruby system and in situ using the Pt pressure calibration (50). Because the Pt peaks were relatively weak due to the small amount of Pt in the starting material, here we report both the ruby and Pt pressures.

Pressure Uncertainty. The precision in measuring the ruby pressure is estimated to be ±0.5 GPa, whereas for Pt pressures, uncertainty is estimated to be of the order 1 to 2 GPa due to the weak nature of the Pt peaks. Another source of

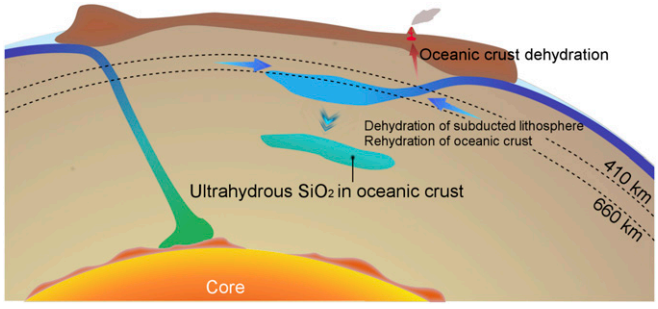

Fig. 3. Transporting water into the lower mantle by ultrahydrous SiO_2. Dehydration of basaltic crust produces melting in the mantle wedge beneath island arcs and effectively dehydrates the crust. However, colder slabs may transport water in subducted mantle lithosphere to transition zone depths where dehydration occurs. Infiltration of fluids or melts through the crust may rehydrate stishovite in the crust to form ultrahydrous stishovite, which can then be transported into the deep lower mantle.

pressure uncertainty is nonhydrostatic stress, which also can affect the measurement of stishovite unit cell volumes. As the ruby pressures are measured away from the heated spot, they may be subject to errors introduced by the stress gradient across the sample. Pt pressures are measured at the place where diffraction is taken and therefore, are more reliably linked to the stishovite unit cell volumes. We performed XRD mapping over the sample after the final heating to estimate the pressure gradient. In an XRD pattern taken close to the heating spot (*SI Appendix*, Fig. S1), the Pt pressure is about 6 GPa higher than the ruby pressure, but this difference varied systematically in the 2 runs as a function of temperature (Fig. 2). The variations in the pressure range in Runs 1 and 2 are 27 to 37 and 43 to 58 GPa, respectively, with pressure increasing after each heating. For stishovite, differential stress results from both the intrinsic lattice anisotropy and the nonhydrostatic conditions. The former is directly related to the tetragonal unit cell of stishovite and was previously quantified by a radial XRD, which showed that the differential stress is ~4.5 GPa below 40 GPa and sharply decreases as it approaches 50 GPa (51).

Analytical Techniques. The diamond anvil cell (DAC) samples, after heated, were prepared for electron microprobe analysis (EMPA) using a focused ion beam (FIB; 30 kV, Ga+ ions, Auriga; Zeiss Instruments) at the Geophysical Laboratory, Carnegie Institution for Science, Washington, DC, which follows the method of ref. 52. Nano- to milliscale milling from the edge of the DAC sample to the heated spot until the quenched silicate phase (stishovite) was exposed and surrounded by iron oxide. A smooth and flat surface was prepared using a 2-nA beam for chemical composition analysis and energy-dispersive spectroscopy mapping. Experimental run products were polished by an FIB for back-scattered electron imagery used to assess the texture and mineralogy (*SI Appendix*, Fig. S2) and then, Ir coated for EMPA. The heating spots of the samples were analyzed by using a JEOL 8530F field emission microprobe at the Geophysical Laboratory, Carnegie Institution for Science. We used 2 different focused beams of 1- and 2-μm diameters for the silicate phase and iron oxide and for the unheated area, respectively. Analyses were done using an accelerating voltage of 15 kV and a beam current of 20 nA. Analyses were calibrated against primary standards of enstatite glass (Si) and basalt 812 glass (Fe). Compositions of the silicate phase and iron oxide (contained within and surrounding each heating spot) reported here are based on 1 to 7 analyses per phase. The EMPA data of DAC samples are shown in *SI Appendix*, Table S3.

Data Availability. The authors declare that all relevant data supporting this study are available within the paper and *SI Appendix* or available on request from the corresponding authors.

ACKNOWLEDGMENTS. We acknowledge Jinfu Shu, Emma Bullock, Suzy Vitale, Lili Zhang, Dongzhou Zhang, and Jingui Xu for experimental assistance and measurements help. This work was performed at HPCAT (Sector 16), Advanced Photon Source (APS), Argonne National Laboratory (ANL). HPCAT operations are supported by the Department of Energy (DOE) National Nuclear Security Administration (NNSA)'s Office of Experimental Sciences. The APS is a US DOE Office of Science User Facility operated for the DOE Office of Science by Argonne National Laboratory under Contract DE-AC02-06CH11357. XRD measurements were performed at the 16ID-B of HPCAT and 13BM-C of GeoSoilEnviroCARS (GSECARS), APS, ANL; the 13BM-C operation is supported by Consortium for Materials Properties Research in Earth Sciences through the Partnership for Extreme Crystallography project under NSF Cooperative Agreement EAR 11-57758. Y.L. and H.-K.M. are supported by NSF Grant EAR-1722515. The Center for High Pressure Science and Technology Advanced Research is supported by National Science Foundation of China Grants U1530402 and U1930401. Part of the experiment was performed at the BL15U1 beamline, Shanghai Synchrotron Radiation Facility in China.

1. T. Inoue, Effect of water on melting phase relations and melt composition in the system Mg_2SiO_4–$MgSiO_3$–H_2O up to 15 GPa. *Phys. Earth Planet. Inter.* **85**, 237–263 (1994).
2. S. Karato, M. S. Paterson, J. D. FitzGerald, Reology of synthetic olivine aggregates: Influence of grain size and water. *J. Geophys. Res.* **91**, 8151–8176 (1986).
3. Y. Lin, E. J. Tronche, E. S. Steenstra, W. van Westrenen, Evidence for an early wet Moon from experimental crystallization of the lunar magma ocean. *Nat. Geosci.* **10**, 14–18 (2017).
4. T. Yoshino, T. Matsuzaki, S. Yamashita, T. Katsura, Hydrous olivine unable to account for conductivity anomaly at the top of the asthenosphere. *Nature* **443**, 973–976 (2006).
5. D. L. Lakshtanov *et al*., The post-stishovite phase transition in hydrous alumina-bearing SiO_2 in the lower mantle of the earth. *Proc. Natl. Acad. Sci. U.S.A.* **104**, 13588–13590 (2007).
6. B. Schmandt, S. D. Jacobsen, T. W. Becker, Z. Liu, K. G. Dueker, Earth's interior. Dehydration melting at the top of the lower mantle. *Science* **344**, 1265–1268 (2014).
7. E. Boulard *et al*., CO_2-induced destabilization of pyrite-structured FeO_2Hx in the lower mantle. *Natl. Sci. Rev.* **5**, 870–877 (2018).
8. J. Zhang, J. D. Bass, Sound velocities of olivine at high pressures and temperatures and the composition of Earth's upper mantle. *Geophys. Res. Lett.* **43**, 9611–9618 (2016).
9. H. Mao *et al*., When water meets iron at Earth's core–Mantle boundary. *Natl. Sci. Rev.* **4**, 870–878 (2017).
10. E. Ohtani, The role of water in Earth's mantle. *Natl. Sci. Rev.*, 10.1093/nsr/nwz071 (2019).
11. M. Nishi *et al*., Stability of hydrous silicate at high pressures and water transport to the deep lower mantle. *Nat. Geosci.* **7**, 224–227 (2014).
12. M. G. Pamato *et al*., Lower-mantle water reservoir implied by the extreme stability of a hydrous aluminosilicate. *Nat. Geosci.* **8**, 75–79 (2015).
13. M. J. Walter *et al*., The stability of hydrous silicates in Earth's lower mantle: Experimental constraints from the systems MgO–SiO_2–H_2O and MgO–Al_2O_3–SiO_2–H_2O. *Chem. Geol.* **418**, 16–29 (2015).
14. N. Bolfan-Casanova, H. Keppler, D. C. Rubie, Water partitioning between nominally anhydrous minerals in the MgO–SiO_2–H_2O system up to 24 GPa: Implications for the distribution of water in the Earth's mantle. *Earth Planet. Sci. Lett.* **182**, 209–221 (2000).
15. H. Skogby, "Water in natural mantle minerals. I. Pyroxenes" in *Water in Nominally Anhydrous Minerals*, H. Keppler, J. R. Smyth, Eds. (Reviews in Mineralogy & Geochemistry, de Gruyter, 2006), vol. 62, pp. 155–167.
16. A. Beran, E. Libowitzky, "Water in natural mantle minerals. II. Olivine, garnet, and accessory minerals" in *Water in Nominally Anhydrous Minerals*, H. Keppler, J. R. Smyth, Eds. (Reviews in Mineralogy & Geochemistry, de Gruyter, 2006), vol. 62, pp. 169–191.
17. K. D. Litasov *et al*., High hydrogen solubility in Al-rich stishovite and water transport in the lower mantle. *Earth Planet. Sci. Lett.* **262**, 620–634 (2007).
18. K. Spektor *et al*., Ultrahydrous stishovite from high-pressure hydrothermal treatment of SiO_2. *Proc. Natl. Acad. Sci. U.S.A.* **108**, 20918–20922 (2011).
19. K. Mibe, T. Yoshino, S. Ono, A. Yasuda, T. Fujii, Connectivity of aqueous fluid in eclogite and its implications for fluid migration in the Earth's interior. *J. Geophys. Res.* **108**, 2295 (2003).
20. P. E. van Keken, B. R. Hacker, E. M. Syracuse, Subduction factory. 4. Depth-dependent flux of H_2O from subducting slabs worldwide. *J. Geophys. Res. Solid Earth* **116**, B01401 (2011).
21. T. Plank, K. A. Kelley, M. M. Zimmer, E. H. Hauri, P. J. Wallace, Why do mafic arc magmas contain ~4 wt% water on average? *Earth Planet. Sci. Lett.* **364**, 168–179 (2013).
22. P. Ulmer, V. Trommsdorff, Serpentine stability to mantle depths and subduction-related magmatism. *Science* **268**, 858–861 (1995).
23. K. D. Litasov, E. Ohtani, Stability of various hydrous phases in CMAS pyrolite–H_2O system up to 25 GPa. *Phys. Chem. Miner.* **30**, 147–156 (2003).
24. D. L. Kohlstedt, H. Keppler, D. C. Rubie, Solubility of water in the α, β, and γ phases of $(Mg,Fe)_2SiO_4$. *Contrib. Mineral. Petrol.* **123**, 345–357 (1996).
25. S. Ono, E. Ito, T. Katsura, Mineralogy of subducted basaltic crust (MORB) from 25 to 37 GPa, and chemical heterogeneity of the lower mantle. *Earth Planet. Sci. Lett.* **190**, 57–63 (2001).
26. K. Hirose, N. Takafuji, N. Sata, Y. Ohishi, Phase transition and density of subducted MORB crust in the lower mantle. *Earth Planet. Sci. Lett.* **237**, 239–251 (2005).
27. K. J. Kingma, R. E. Cohen, J. Russell, H. K. Mao, Transformation of stishovite to a denser phase at lower-mantle pressures. *Nature* **374**, 243–245 (1995).
28. R. A. Fischer *et al*., Equations of state and phase boundary for stishovite and $CaCl_2$-type SiO_2. *Am. Mineral.* **103**, 792–802 (2018).
29. A. E. Gleason *et al*., Ultrafast visualization of crystallization and grain growth in shock-compressed SiO_2. *Nat. Commun.* **6**, 8191 (2015).
30. C. Nisr, S. H. Shim, K. Leinenweber, A. Chizmeshya, Raman spectroscopy of water-rich stishovite and dense high-pressure silica up to 55 GPa. *Am. Mineral.* **102**, 2180–2189 (2017).
31. D. Andrault, R. J. Angel, J. L. Mosenfelder, T. L. Bihan, Equation of state of stishovite to lower mantle pressures. *Am. Mineral.* **88**, 301–307 (2003).
32. J. S. Pigott *et al*., High-pressure, high-temperature equations of state using nano-fabricated controlled-geometry Ni/SiO_2/Ni double hot-plate samples. *Geophys. Res. Lett.* **42**, 239–247 (2015).
33. K. Spektor *et al*., Formation of hydrous stishovite from coesite in high pressure hydrothermal environments. *Am. Mineral.* **101**, 2514–2524 (2016).
34. C. Nisr *et al*., Phase transition and equation of state of dense hydrous silica up to 63 GPa. *J. Geophys. Res. Solid Earth* **122**, 6972–6983 (2017).
35. A. R. Pawley, P. F. McMillan, J. R. Holloway, Hydrogen in stishovite, with implications for mantle water content. *Science* **261**, 1024–1026 (1993).
36. J. I. Chung, H. Kagi, High concentration of water in stishovite in the MORB system. *Geophys. Res. Lett.* **29**, 2020 (2002).
37. W. R. Panero, L. R. Benedetti, R. Jeanloz, Transport of water into the lower mantle: Role of stishovite. *J. Geophys. Res.* **108**, 2039 (2003).
38. N. Bolfan-Casanova, Water in the Earth's mantle. *Mineral. Mag.* **69**, 229–257 (2005).
39. N. Bolfan-Casanova, H. Keppler, D. C. Rubie, Water partitioning at 660 km depth and evidence for very low water solubility in magnesium silicate perovskite. *Geophys. Res. Lett.* **30**, 1905 (2003).

40. S. Fu *et al*., Water concentration in single-crystal (Al,Fe)-Bearing bridgmanite grown from the hydrous melt: Implications for dehydration melting at the topmost lower mantle. *Geophys. Res. Lett.* **46**, 10346–10357 (2019).
41. T. Komabayashi, S. Omori, S. Maruyama, Petrogenetic grid in the system MgO-SiO_2-H_2O up to 30 GPa, 1600 °C: Applications to hydrous peridotite subducting into the Earth's deep interior. *J. Geophys. Res.* **109**, B03206 (2004).
42. D. G. Pearson *et al*., Hydrous mantle transition zone indicated by ringwoodite included within diamond. *Nature* **507**, 221–224 (2014).
43. E. M. Smith *et al*., Blue boron-bearing diamonds from Earth's lower mantle. *Nature* **560**, 84–87 (2018).
44. Y. Tsuchida, T. Yagi, A new, post-stishovite high-pressure polymorph of silica. *Nature* **340**, 217–220 (1989).
45. M. M. Hirschmann, R. Dasgupta, The H/C ratios of Earth's near-surface and deep reservoirs, and consequences for deep Earth volatile cycles. *Chem. Geol.* **262**, 4–16 (2009).
46. A. P. Jephcoat, H. K. Mao, P. M. Bell, *Hydrothermal Experiment Techniques* (Wiley-Interscience, 1987), chap. 11.
47. H. Yuan, L. Zhang, In situ determination of crystal structure and chemistry of minerals at Earth's deep lower mantle conditions. *Matter Radiat. Extremes* **2**, 117–128 (2017).
48. Y. Meng, G. Shen, H. K. Mao, Double-sided laser heating system at HPCAT for in situ x-ray diffraction at high pressures and high temperatures. *J. Phys. Condens. Matter* **18**, S1097–S1103 (2006).
49. T. J. B. Holland, S. A. T. Redfern, Unit cell refinement from powder diffraction data: The use of regression diagnostics. *Min. Mag. (Lond.)* **61**, 65–77 (1997).
50. Y. Fei *et al*., Toward an internally consistent pressure scale. *Proc. Natl. Acad. Sci. U.S.A.* **104**, 9182–9186 (2007).
51. S. R. Shieh, T. S. Duffy, B. Li, Strength and elasticity of SiO_2 across the stishovite-$CaCl_2$-type structural phase boundary. *Phys. Rev. Lett.* **89**, 255507 (2002).
52. C. R. M. Jackson, N. R. Bennett, Z. Du, E. Cottrell, Y. Fei, Early episodes of high-pressure core formation preserved in plume mantle. *Nature* **553**, 491–495 (2018).